Plasma Physics and Technology **XX**(X):1–7, 2017

MECHANISMS RESPONSIBLE FOR ARC COOLING IN DIFFERENT GASES IN TURBULENT NOZZLE FLOW

Y.GUO[a], H.ZHANG[a], Y.YAO[a], Q.ZHANG[b], J.D.YAN[b,*]

[a] *Pinggao Group Co. Ltd., Pingdingshan City, Henan, China, 467001*
[b] *Department of Electrical Engineering and Electronics, the University of Liverpool, Liverpool L69 3GJ, the U.K.*
[*] yaneee@liverpool.ac.uk

Abstract. A high voltage gas blast circuit breaker relies on the high speed gas flow in a nozzle to remove the energy due to Ohmic heating at high current and to provide strong arc cooling during the current zero period to interrupt a fault current. The physical mechanisms that are responsible for the hugely different arc cooling capabilities of two gases (SF_6 and air) are studied in the present work and important gas material properties controlling the cooling strength identified.

Keywords: SF_6 replacement, SF_6 alternative gases, switching arc.

1. Introduction

SF_6 has long been exclusively used in gas blast circuit breakers at voltage levels above 245 kV because of its excellent dielectric strength and current interruption capability. It is however a strong greenhouse gas with a Global Warming Potential of 23,500 [1]. There has been increasing worldwide effort in the last 10 years to search for alternatives gases that can replace SF_6 for high current switching. Most of the work carried out so far has however focused on the dielectric performance of potential gases such as CF_3I, $C_5F_{10}O$ and C_4F_7N and their mixtures with CO_2 [2][3][4], operating temperature of gas mixture [5], gas decomposition [6] and toxicity [6]. There is a limited amount of experimental work on the interruption capability of the potential alternative gases [7][8][9], but little work towards a quantitative understanding of the mechanisms responsible for the hugely different interruption capabilities of different gases.

The present work is aimed towards a quantitative explanation of the relevant importance of different energy exchange mechanisms participating in the arc cooling process and the identification of the causes that control their relevant cooling strength. The arc model will be first introduced with a discussion on the choice of the turbulent models. This is followed by a verification of the model using existing experimental results for which test conditions are known. The temperature distribution of the arc column and the energy exchange fluxes due to thermal conduction (including turbulent enhanced heat exchange), convection and radiation will be analysed to identify the mechanisms through which different gases produce different arc cooling effect. It is expected that the findings will be directly relevant to the composition or selection of SF_6 alternative gases by relating the interruption capability of a gas to its material properties.

2. Arc model

2.1. Governing equation

Local thermodynamic equilibrium (LTE) is a commonly accepted assumption for the plasma state in switching arcs. Gas flow inside and around the arc column which is confined in a nozzle is turbulent in nature and can be described by the time averaged Navier-Stokes equations modified to take into account the effects of Ohmic heating, radiation transfer and electromagnetic field. By assuming axisymmetry for the switching arc, the conservation equations are given below in cylindrical coordinates:

$$\frac{\partial(\rho\phi)}{\partial t} + \frac{1}{r}\frac{\partial[r\rho v\phi - r\Gamma_\phi \frac{\partial\phi}{\partial r}]}{\partial r} + \frac{\partial[\rho w\phi - \Gamma_\phi \frac{\partial\phi}{\partial z}]}{\partial z} = S_\phi \quad (1)$$

where ϕ is the dependent variable and ρ the gas density. v and w are respectively the radial and axial velocity components. The source terms (S_ϕ) and the diffusion coefficients (Γ_ϕ) are listed in Table 1 where all notations have their conventional meaning. The subscript l denotes the laminar part of the exchange coefficient and t the turbulent part. Viscous heating due to molecular and turbulent stresses is given in the source term for the enthalpy equation (Table 1).

The equation of state and the thermodynamic properties and transport coefficients including electrical conductivity are determined by the gas temperature and pressure only under LTE and usually given in the form of data tables. These data are taken from [10] for SF_6, and [11][12] for air.

For low current nozzle arc, the radial component of electrical field is negligible in comparison with the axial component and the radial variation of the axial component is much smaller than its magnitude. Therefore, the axial electrical field is considered to be constant over the arc cross-section, which can be calculated by the simplified Ohmic law

Equation	ϕ	Γ_ϕ	S_ϕ
Continuity	1	0	0
Z-momentum	w	$\mu_l+\mu_t$	$-\frac{\partial p}{\partial z}$
R-momentum	v	$\mu_l+\mu_t$	$-\frac{\partial p}{\partial r}-(\mu_l+\mu_t)\frac{v}{r^2}$
Enthalpy	h	$\frac{k_l+k_t}{C_p}$	$\frac{dp}{dt}+\sigma E^2-q+(\mu_l+\mu_t)\{2[(\frac{\partial v}{\partial r})^2+\frac{v^2}{r^2}+(\frac{\partial w}{\partial z})^2]+(\frac{\partial v}{\partial z}+\frac{\partial w}{\partial z})^2\}$

Table 1. Terms in governing equations (1).

$$i = E\int_0^\infty \sigma 2\pi r dr \qquad (2)$$

where i is the instantaneous current and σ the electrical conductivity.

For an axisymmetric arc with monotonically decreasing radial temperature profile, radiation transport can be calculated with the approximate model of Zhang et al. [13] which calculates the volumetric radiative energy loss in the arc core (from axis up to R_{83} which is the radius corresponding to 83% of the axis temperature) based on the concept of net emission coefficient (NEC) and radiation absorption (from R_{83} to R_{4K} which is the radius corresponding to 4000 K) in the surrounding gas layer. The NEC values as a function of pressure and temperature under LTE is from [14] for SF_6 and [15][16] for air and nitrogen. The NEC is defined for an isothermal cylindrical column of infinite length. In switching arc applications, the arc column is never isothermal. Therefore the use of the NEC is only approximate and the definition of the arc radius will affect the accuracy of the calculation of the emitted power from the arc core. By comparing with the measured arc temperature, it was found that the NEC data based on an emission radius defined as $0.5(R_{83}+R_{4K})$ needs to be multiplied by a factor of 2.5 to achieve good agreement. This approximate model has been proven sufficiently accurate in the modelling of nozzle arcs. The percentage of the radiation flux from the arc core that is absorbed at the arc edge is a parameter in the approximate model. It is 80% for SF_6 and 60% for air based on previous studies.

2.2. Turbulence models

There are numerous turbulence models, however there is no general theoretical guidance regarding the choice of turbulence models for arcs in supersonic flow. Prandtl mixing length model has achieved considerable success in predicting turbulent arc behavior. The standard k-Epsilon model with the default values for the five parameters and two of its variants (the renormalization group, commonly known as the RNG model and Chen-Kim model) have been used for the modelling of turbulent arc flow in circuit breakers with contradictory claims regarding their successes. The Prandtl mixing length model relates the turbulence length scale to the width of the jet which marks the boundary of the high velocity core. It is calculated by

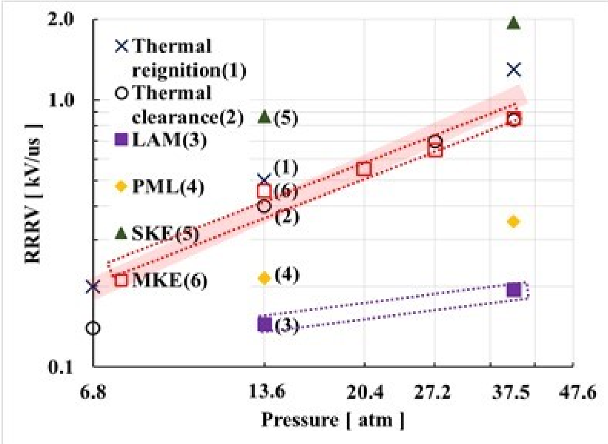

Figure 1. Predicted critical rate of rise of recovery voltage (RRRV) of air as a function of upstream stagnation pressure with $di/dt = 13.5\ A/\mu s$. Simulation conditions are identical to those used in the experiment [9].

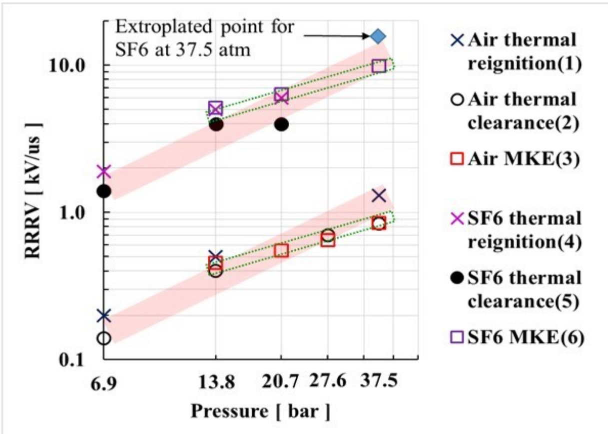

Figure 2. Predicted RRRV for SF_6 and air as a function of upstream stagnation pressure with $di/dt = 13.5\ A/\mu s$. Experimental results are from [9].

$$\lambda_c = cr_\delta = c\sqrt{\int_0^\infty (1-\frac{T_\infty}{T})2rdr} \qquad (3)$$

where T_∞ is the temperature near the nozzle wall where the radial temperature gradient is negligible. c is a turbulence parameter the value of which is found by the best fit between model prediction and experimental results. The eddy viscosity is related to the turbulence length scale and the mean velocity

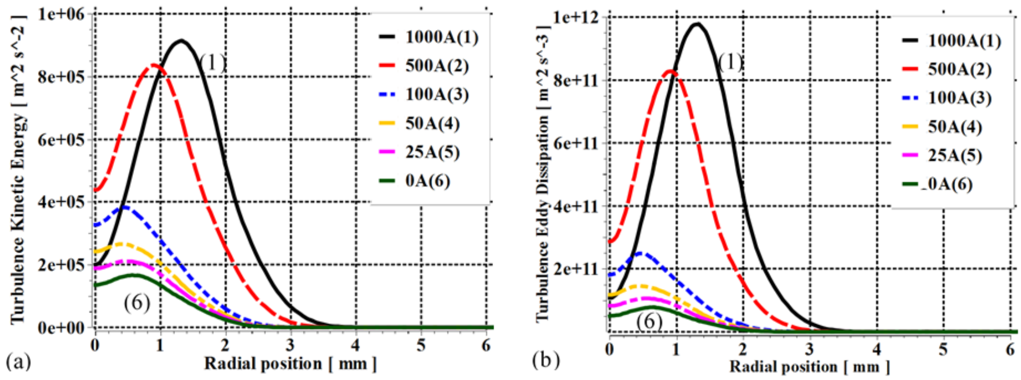

Figure 3. Radial distribution of turbulence kinetic energy and its dissipation rate in air arc at the axial location of 17 mm downstream the nozzle throat [9].

gradient by

$$\mu_t = \rho \lambda_c^2 \left(\left| \frac{\partial w}{\partial r} \right| + \left| \frac{\partial v}{\partial z} \right| \right) \quad (4)$$

The existence of turbulence eddies in the main flow enhances the energy exchange process when a temperature gradient exists. In analogue to thermal conduction, the turbulent counterpart to the laminar thermal conductivity is related to the eddy viscosity through a unit Prandtl number by

$$Pr_t = \frac{\mu_t}{(k_t/C_p)} = 1 \quad (5)$$

Thus we are able to quantitatively account for the effect of turbulent cooling by the use of a turbulent thermal conductivity k_t. The standard K-Epsilon model (SKE) and its variants consider the conversion of the main flow kinetic energy into the chaotic turbulence kinetic energy, k, as well as the destroy of turbulence eddies through a turbulence kinetic energy dissipation rate, ε:

$$\frac{\partial(\rho k)}{\partial t} + \nabla \cdot (\rho \mathbf{V} k - \frac{\rho \nu_t}{\sigma_k} \nabla k) = \rho (P_k - \varepsilon) \quad (6)$$

$$\frac{\partial(\rho \varepsilon)}{\partial t} + \nabla \cdot (\rho \overrightarrow{V} \varepsilon - \frac{\rho \nu_t}{\sigma_\varepsilon} \nabla \varepsilon) = \rho \frac{\varepsilon}{k} (C_{1e} P_k - C_{2e} \varepsilon) \quad (7)$$

where P_k represents the generation of turbulence kinetic energy due to the existence of mean flow velocity gradient, which is given by

$$P_k = \nu_t [2(\frac{\partial w}{\partial z})^2 + 2(\frac{\partial v}{\partial r})^2 + 2(\frac{v}{r})^2 + (\frac{\partial w}{\partial r} + \frac{\partial v}{\partial z})^2] \quad (8)$$

The turbulence length and velocity scales are respectively defined as $\lambda_c \propto k^{1.5/\varepsilon}$ and $V_c \propto k^{0.5}$.

The eddy viscosity is expressed as

$$\mu_t = \rho C_\mu \frac{k^2}{\varepsilon} \quad (9)$$

There are altogether five model constants in the k-Epsilon model with the default values of $\sigma_k = 1.0$, $\sigma_\varepsilon = 1.3$, $C_{1e} = 1.44$, $C_{2e} = 1.92$ and $C_\mu = 0.09$. By calibrating this model and examining its validity against experimental results, it has been found that acceptable agreement can be achieved by adjusting C_{1e} from 1.44 to 1.62. For comparison, the Chen-Kim K-Epsilon model and the RNG K-Epsilon model were also used in the calibration process [17]. Results shown in Figure 1 show that the prediction made by laminar flow assumption is simply too low. The Prandtl mixing length model (PML) also produces interruption capability that is significantly below the measurement while the standard K-Epsilon model (SKE) gives much higher prediction. However the modified K-Epsilon model (MKE) gives acceptable agreement for both DC at different current [18] as well as transient arcs at different upstream pressure [9]. We thus have confidence in the MKE model to represent the turbulence effect in the arcing process and the results using the MKE model will be studied to identify the dominant mechanisms responsible for the cooling effect of different gases.

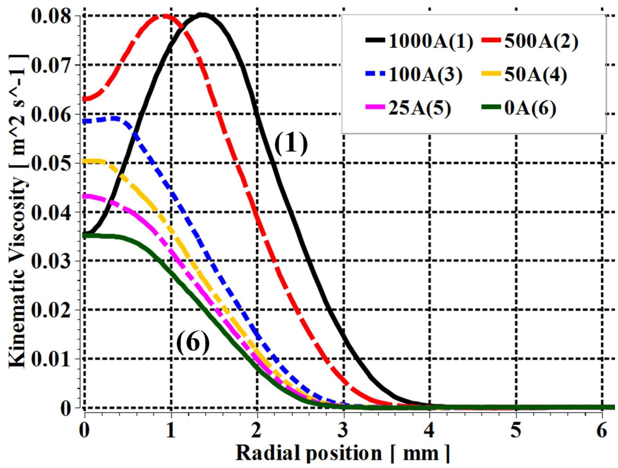

Figure 4. Radial distribution of turbulent kinematic viscosity in air arc at the axial location of 17 mm downstream the nozzle throat [9].

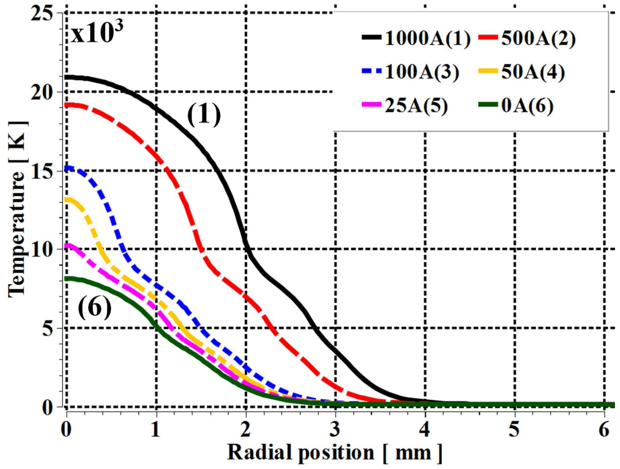

Figure 5. Radial distribution of air arc temperature at the axial location of 17 mm downstream the nozzle throat [9].

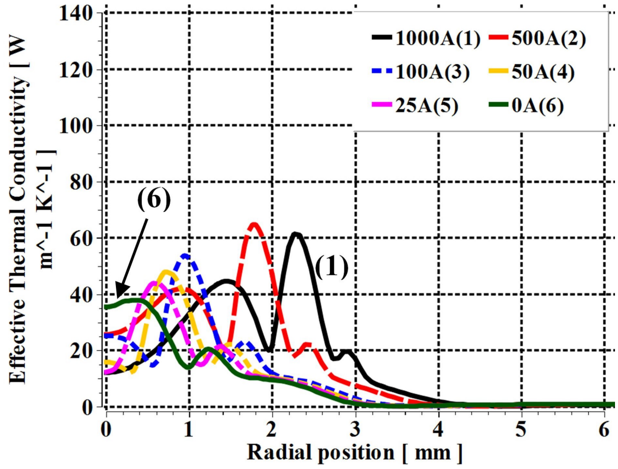

Figure 6. Radial distribution of the effective turbulent thermal conductivity in air arc at the axial location of 17 mm downstream the nozzle throat [9].

3. Comparative analysis of the energy exchange mechanisms in different gases

3.1. Difference in interruption capability of SF_6 and air

It is well know that the current interruption capability of SF_6 is much higher than that of the air, as experimentally proved by Frind and Rich [9] in a supersonic nozzle. Figure 2 shows the relative largeness of the interruption capability in terms of RRRV. Different from the dielectric strength which is a well-defined material property that only depends on the state of the gas, the current interruption capability of a gas not only depends on the type of gas, but also depends on the flow field, which explains the difference in interruption capabilities obtained in different experiments. For example, the interruptible RRRV ratio of SF_6 to air in a supersonic nozzles with a fixed upstream pressure of 37.5 bar and a di/dt immediately before current zero of 13.5 A/μs is 1 : 0.1[9] whereas the interruptible di/dt (immediately before current zero) ratio obtained from a model circuit breaker is 1 : 0.28 [8].

The difference in interruption capability between SF_6 and air is also predicted by our arc model (Figure 2) where good agreement with measurement is observed. Results in Figure 1 also shows that despite the interruption capability of air is significantly lower than SF_6, turbulence is still important because without including turbulence the predicted RRRV is 30% or even lower than the measured values when the upstream pressure is higher than 13.6 bar.

3.2. The role of turbulence

The presence of turbulence eddies in the flow promotes momentum and energy exchange by increasing the effective viscosity and thermal conductivity of the gas. Since the turbulence kinetic energy generation term (Equation (8)) depends on the velocity gradient, it is expected that the kinematic viscosity will be largest at the arc edge where the velocity profile is the steepest. Figure 3 shows that the radii at which the maximum value of the turbulence kinetic energy and its dissipation rate occur are the same and decrease when the current linearly ramps down towards current zero. At 1 kA and 500 A, the radius of the arc core is larger than 1 mm. It is apparent that diffusion fails to spread the turbulence towards the centre of the arc column when convection in the axial direction is strong and the radial gradient of the axial velocity becomes smaller towards the arc centre. As a result turbulent kinematic viscosity reaches its maximum at the arc edge (Figure 4).

When the current reduces towards its zero point, the size of the arc core becomes smaller (Figure 5) and the maximum kinematic viscosity is the largest at the arc centre (Figure 4). It must however be noted that turbulence enhanced energy transfer in terms of the turbulent thermal conductivity as given in Equation (5) is the product of density, specific heat at constant pressure and the turbulent kinematic viscosity. Since the specific heat represents the energy density per unit mass, it directly affects the net energy exchange flux when there exists a temperature gradient. Thus the effective turbulent thermal conductivity has a more complex radial distribution, as shown in Figure 6. It is no longer monotonic and has two peaks. This is the result of the multiple peaks in the specific heat as a function of temperature. The product of density and specific heat (hereafter referred to as ρC_p for convenience) of three gases is shown in Figure 7 where there are two peaks above 4000 K (air at this temperature no longer conducts electricity).

Since the arc column is surrounded by cold gas, the temperature of the gas has to change from a high value at the arc centre to the cold gas temperature. The existence of radial temperature gradient enables the turbulent thermal conductivity to have an important role in shaping the radial temperature profile despite

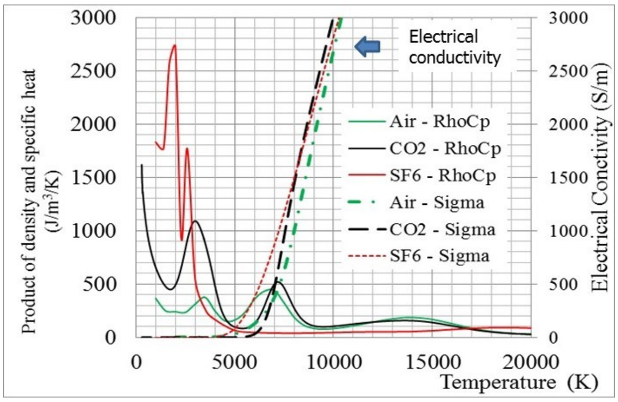

Figure 7. Product of density and specific heat of three gases as a function of temperature at 1 bar.

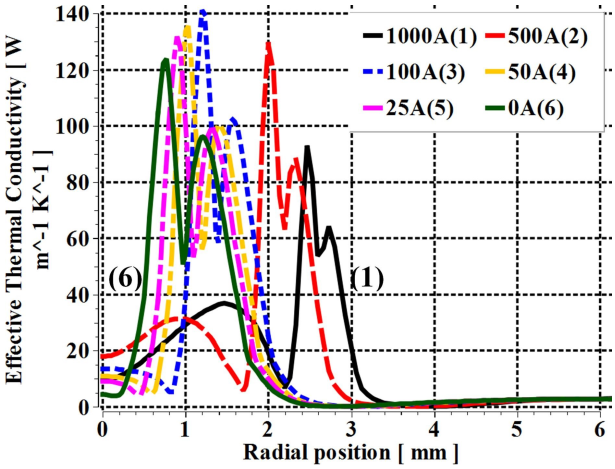

Figure 8. Radial distribution of the effective turbulent thermal conductivity in SF_6 arc at the axial location of 17 mm downstream the nozzle throat [9].

convection and radiation have also influence on it. Results in Figure 5 clearly show that the non-monotonic radial distribution of the effective turbulent thermal conductivity leads to the inflection points as labelled. From Figure 8, there will be two inflection points in the radial temperature profile as long as the arc centre temperature is high than 10,000 K. The immediate consequence of the existence of the inflection points is that the arc column (electricity conduction region) becomes larger in size.

For comparison, SF_6 has consistently low ρC_p in the temperature range above 4,000 K when it starts to become electrically conductive (rapidly increasing electrical conductivity). The very high ρC_p below 4,000 K means highly efficient energy removal in the cooler surrounding gas so below 4,000 K the radial temperature gradient would be small. The low ρC_p above 4,000 K means the temperature gradient has to be large to maintain a radial energy flux that the surrounding cooler gas can absorb. The distribution of the effective turbulent thermal conductivity for SF_6 under identical arcing conditions is given in Figure 8 and the radial temperature in Figure 9. The only inflection point in the arc column for SF_6 is that

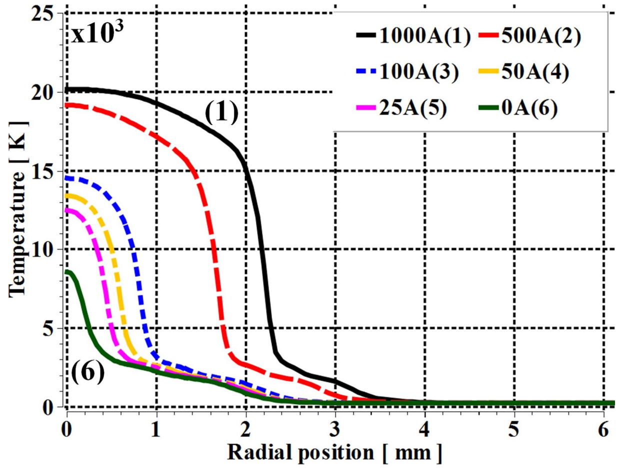

Figure 9. Radial distribution of SF_6 arc temperature at the axial location of 17 mm downstream the nozzle throat [9].

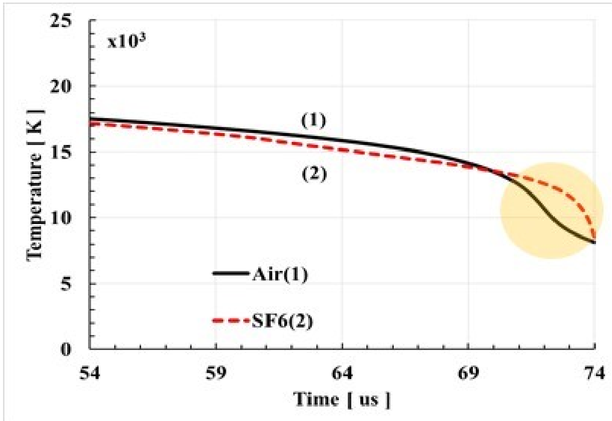

Figure 10. Variation of the axis temperature at the axial location of 17 mm downstream the nozzle throat [9]. The current at 54 μs is 270 A, nearly reaching 0 A at 74 μs.

near the conducting temperature of SF_6 (4,000 K), i.e. close to the cooler surrounding gas. This means that because the ρC_p peaks for SF_6 lies below the conducting temperature while that of the air lies above the conducting temperature, the arc column of air arc is therefore broadened.

3.3. Energy exchange mechanisms leading to different current interruption capability

Arc cooling depends on the energy removal rate from the conducting column, or the arc column. At high current where Ohmic heating is strong, energy removal heavily relies on radiation and convection. However when the arcing current rapidly decreases towards its zero point, the arc column rapidly shrinks and turbulence enhanced thermal conduction becomes important or even dominant. Since the energy transfer mechanisms are closely coupled through the conservation equations, it is impossible to obtain analytic solution to the conservation equations. An approximate order of magnitude analysis shows that the char-

Gas	Current (A)	Radial thermal conduction	Radial convection	Radiation	Total radial cooling (%)	Axial cooling (%)
Air	500	13.6	-22.3	13.6	5.0	86.7
	50	20.1	11.6	1.3	33	57.4
	25	22.2	20.8	0.4	43.4	50
SF_6	500	33.9	0	9.7	43.5	47.7
	50	45	27.3	4.8	77	20.5
	25	45.2	35.1	6.2	86.5	12.6

Table 2. Percentage weighting of different energy exchange mechanisms for the whole arc column in SF_6 and air. The sum of Ohmic heating and reduction rate of the energy storage in the arc column is taken as 100%.

acteristic time for cooling by different mechanisms points to the relationship of $\tau_{r,tur} \sim r_a$ for radial turbulent cooling, $\tau_{r,con} \sim r_a/v_b$ for radial convective cooling where v_b is a positive radial velocity at the conduction boundary of the arc column, and $\tau_{z,con}$ does not depends on r_a for axial convective cooling (r_a is the conducting column radius). This means energy removal across the radial boundary of the arc column becomes stronger when the arc radius decreases while the axial convective cooling is not sensitive to the change in arc radius.

A broadened arc column such as in air will lead to larger radial characteristic cooling time, thus lower RRRV values in comparison with SF_6 under identical flow conditions. Results in Table 2 clearly show that at 500 A, radial convection does not contribute to the cooling process instead it brings energy into the arc column. Turbulent enhanced radial thermal conduction already takes away 34% of the total energy loss in SF_6 arc at 500 A while in air arc it is less than 14%. This is directly a consequence of the broadening of the arc column. Near current zero (25 A), the total radial cooling effect accounts for 86% of the total cooling in SF_6 while for air it is only 43%. The difference is expected to be even larger when the current further reduces. Results in Figure 10 affirm our findings where the axis temperature in the SF_6 arc starts to reduce much more rapidly than the air arc when the current approaches zero due to much stronger turbulent cooling effect of SF_6.

4. Conclusion

A detailed study into the causes of SF_6's excellent current interruption capability in comparison with air has been carried out. It is shown that the huge difference in the interruption capability of SF_6 and air, when the arc is quenched in a supersonic nozzle, originates from the difference in their material properties, or the product of density and specific heat at constant pressure as a function of temperature. More specifically, it is the ρC_p peaks of air at temperatures above the conducting temperature (4,000 K) that broadens the arc column, consequently reduces the effectiveness of turbulent cooling. This is in contrast to SF_6 whose large ρC_p peak is below the conducting temperature. The consistently low ρC_p value of SF_6 above the conducting temperature leads to a sharp edge of the arc column and a smaller arc radius, enabling efficient turbulent cooling. Therefore, for the purpose of selecting or chemically composing SF_6 alternative gas or gas mixtures, one of the criteria will be that the ρC_p values above their conducting temperature should be consistently low and that below the conducting temperature should be high.

References

[1] Fifth assessment report (ar5) of the intergovernmental panel on climate change (ipcc), 2013.

[2] H Katagiri, H Kasuya, H Mizoguchi, and S Yanabu. *IEEE Transactions on Dielectrics and Electrical Insulation*, 15(5), 2008.

[3] Houssem Eddine Nechmi, Abderrahmane Beroual, Alain Girodet, and Paul Vinson. *IEEE Transactions on Dielectrics and Electrical Insulation*, 23(5):2587–2593, 2016.

[4] P Simka and N Ranjan. In *19th International Symposium on High Voltage Engineering, Pilsen, Czech Republic*, pages 23–28, 2015.

[5] JD Mantilla, N Gariboldi, S Grob, and M Claessens. In *Electrical Insulation Conference (EIC), 2014*, pages 469–473. IEEE, 2014.

[6] Abderrahmane Beroual and Abderrahmane Manu Haddad. *Energies*, 10(8):1216, 2017.

[7] G Frind. *EPRI Report*, 284:5, 1977.

[8] Patrick C Stoller, Martin Seeger, Arthouros A Iordanidis, and George V Naidis. *IEEE Transactions on Plasma Science*, 41(8):2359–2369, 2013.

[9] G Frind and JA Rich. *IEEE Transactions on Power Apparatus and Systems*, (5):1675–1684, 1974.

[10] Leslie S Frost and Richard W Liebermann. *Proceedings of the IEEE*, 59(4):474–485, 1971.

[11] JM Yos. *AVCO Technical Release*, 28, 1967.

[12] PJ Shayler and MTC Fang. *Journal of Physics D: Applied Physics*, 10(12):1659, 1977.

[13] JF Zhang, MTC Fang, and DB Newland. *Journal of Physics D: Applied Physics*, 20(3):368, 1987.

[14] RW Liebermann and JJ Lowke. *Journal of quantitative spectroscopy and radiative transfer*, 16(3):253–264, 1976.

[15] JJ Lowke. *Journal of Quantitative Spectroscopy and Radiative Transfer*, 14(2):111–122, 1974.

[16] PJ Shayler and MTC Fang. *Journal of Physics D: Applied Physics*, 11(12):1743, 1978.

[17] Q Zhang, JD Yan, and MTC Fang. *Journal of Physics D: Applied Physics*, 47(21):215201, 2014.

[18] MTC Fang, S Ramakrishnan, and HK Messerle. *IEEE Transactions on Plasma Science*, 8(4):357–362, 1980.